accepted manuscript
Medical Engineering & Physics

Influence of Flexural Rigidity on Micromotion at the Head-Stem Taper Interface of Modular Hip Prostheses

Henning Haschke[1], Tobias Konow[1], Gerd Huber[1] and Michael M Morlock[1]

[1] Institute of Biomechanics, TUHH Hamburg University of Technology, Germany

Corresponding author:
Henning Haschke
TUHH Hamburg University of Technology
Institute of Biomechanics
Denickestraße 15
21073 Hamburg
Germany
Phone: +49 40 42878 3712
Email: haschke@tuhh.de

Hamburg, November 12th, 2018 (revised March 25th, 2019; accepted March 31st, 2019)

5259 words (body without references), 188 words (abstract)

Abstract

Fretting corrosion as one reason for failure of modular hip prostheses has been associated with micromotion at the head taper junction. Historically the taper diameter was reduced to improve the range of motion of the hip joint. In combination with other developments, this was accompanied by increased observations of taper fretting, possibly due to the reduced flexural rigidity of smaller tapers. The aim of the study was to investigate, how the flexural rigidity of tapers influences the amount of micromotion at the head taper junction.

Three different stem and two different taper designs were manufactured. Experimental testing was performed using three different activity levels with peak loads representing walking, stair climbing and stumbling. The relative motion at the head-stem taper was measured in six degrees of freedom. Micromotion was obtained by subtraction of the elastic deformation derived from monoblock and finite element analysis.

Less rigid tapers lead to increased micromotion between the head and stem, enlarging the risk of fretting corrosion. The influence of the stem design on micromotion is secondary to taper design. Manufacturers should consider stiffer taper designs to reduce micromotion within the head taper junction.

Keywords

Flexural rigidity, micromotion, relative motion, taper interface, taper size, modular hip prostheses

Highlights

- Reduction of taper size and stiffness is a trade-off; micromotion is significantly increased
- Materials with lower elastic modulus can lead to higher micromotion
- High activity levels increase micromotion between prosthesis head and stem
- V40 taper design showed 300% higher micromotion compared to 12/14 tapers
- Instead of smaller tapers a rounded square neck region should be used to increase the range of motion

1. Introduction

The introduction of modular femoral head-stem combinations for total hip arthroplasties (THAs) in the 1980s established several advantages over monoblock designs. A combination of different materials for the head and the stem could be realized, which lead to a variety of advantageous combinations, such as cobalt chrome or ceramic heads on titanium stems. With a broader choice of materials, the head-stem combination could be matched to fit the patients' requirements, such as avoidance of allergic reactions to cobalt chrome or consideration of a high body mass index (BMI). Moreover, the opportunity to take benefit from the adaptation to the patient-specific anatomy concerning the centrum collum-diaphysis angle (CCD), the range of motion (ROM) and femoral offset was also advantageous [1–3].

This modularity was enabled by the introduction of conical modular press fit taper junctions. The connection between the femoral stem and the head is realized by a conical press-fit junction. The characteristics of the taper junction vary among different manufacturers and even for products of the same manufacturer as no standardization of the taper junction is available [4,5]. In general, taper designs (e.g. 10/12, 11/13, 12/14 or 14/16) are labeled according to a theoretical ratio between diameters of two taper cross sections at a distance of 20 mm [6]. For 12/14 taper this would result in a theoretical taper angle of 5 ° 43 ‘ 30”, while the V40 design has a desired taper angle of 5 ° 40 ‘. In this context it has to be noted, that due to individual manufacturing tolerances the female and male tapers angles are different to guaranty a defined but manufacturer specific clamping

77 at either side of the taper. However, the variety of taper designs includes different surface
78 structures, taper lengths and taper angles which can be combined with heads of different
79 sizes and offsets [7]. Yet, evidence-based recommendations regarding optimal taper
80 connection design remain inconclusive and conflicting [8].

81 Innovations were not just introduced for head material and taper design, but also included
82 a large variety of stem designs and materials. More than 100 different stem designs are
83 commercially available [9,10]. Between the different designs, large variations of the
84 length, diameter, shape, surface structure, coating or stem modularity can be found [11].
85 Typically, proximal stem designs can be separated into three prominent groups: round,
86 oval and rounded square neck geometry (Figure 1). The head-neck ratio has a major
87 influence on the impingement behavior [2] and consequently defines the anatomical
88 ROM of the affected joints. Previous research showed that a rounded square/trapezoidal
89 neck design increases the joint mobility in flexion and extension by 20% compared to
90 round neck designs [12]. Furthermore, the combination of small cross-sectioned tapers or
91 necks with large diameter heads increases the ROM without the risk of an impingement
92 [13,14].

93

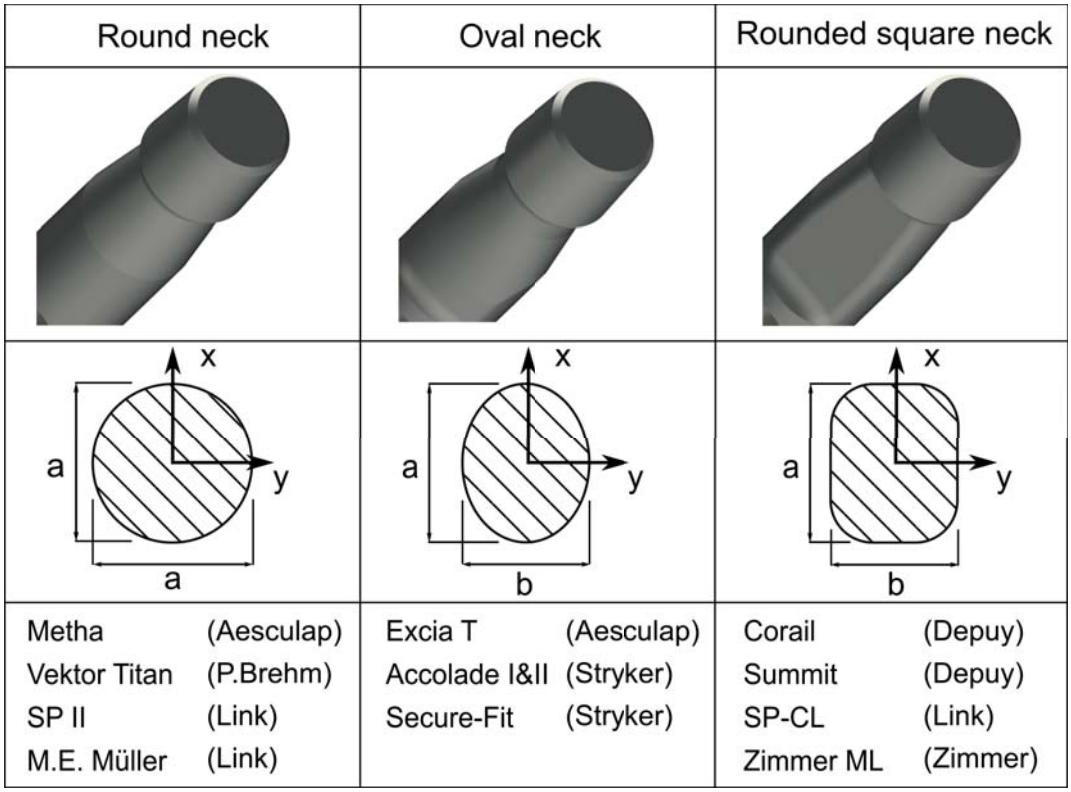

Figure 1: Examples for the geometrical variations in the neck design of modular hip prostheses. Continuously varying cross sections with distance from the proximal taper surface.

As many technical innovations come with a drawback, a new phenomenon was described in the 1990s known as metallosis [15–17]. Several reports of patients with high metal ions blood levels and metal ion accumulation in the surrounding tissue identified the modular taper junction as the root of cause [18–20]. In vivo, the taper junctions are exposed to an exigent environment of the human body such as tissues and body fluids. The national

joint replacement registry of the Australian Orthopaedic Association (AOA) indicated that 25.6 % of all revision surgeries with primary diagnosis osteoarthritis had to be performed due to periprosthetic aseptic loosening [21]. The bulk materials used are themselves highly biocompatible. However, released nano- and microparticles of these materials result in a negative response of the immune system [18]. The result is an increased activation of osteoclasts that can lead to a resorption of the surrounding bone material. This causes a loosening of the femoral stem or the formation of pseudo tumors and necessitates an early revision surgery of the prosthesis [22].

The loosening of the artificial joint is a result of tribological strains promoted by high cyclic loading, e.g. walking activities of 1-2 million steps per year [23,24]. During activities of daily living the artificial joint is loaded with high forces exceeding a multiple of the body weight [25]. Induced by these loadings, micromotion between the taper surfaces of the femoral head and the femoral stem may occur. Micromotion at the head-stem taper junction in combination with the surrounding body fluid may lead to an abrasive release of the corrosive resistant passivation layer (Figure 2) which is known as fretting corrosion [26]. Metal debris resulting from the fretting process, was linked to adverse local tissue reactions, systematic effects on the body and subsequent failure of the implant [18,20].

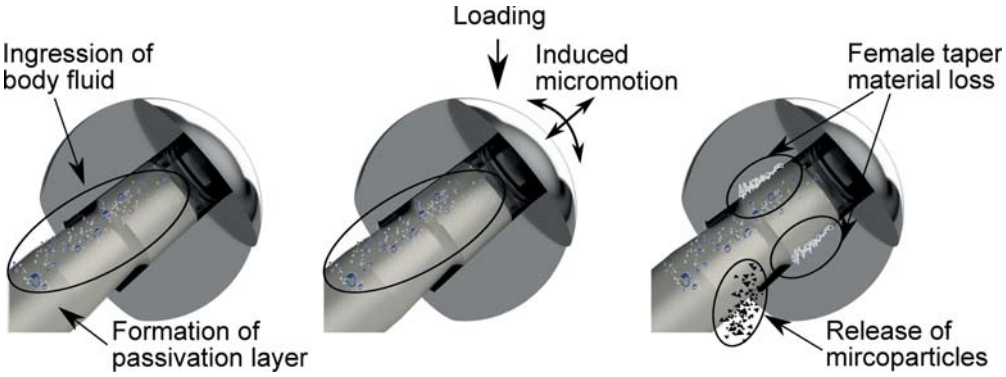

Figure 2: Formation of fretting corrosion and the release of micro particles within the modular taper junction.

The pursuit to eliminate limitations in joint movement, led to the introduction of thinned and shortened taper and neck geometries over several decades from the 1980s to 2010s. Porter et al. found a wide variability in flexural rigidity of various taper designs and described a trend towards shorter and less rigid taper junctions with time [10]. Regardless of the trend, several publications indicate an increased risk for fretting corrosion for less rigid and smaller tapers as well as stems [27–29]. Flexural rigidity as a prevalent risk factor for corrosion is mainly present due to micromotion that is promoted by higher elastic strains [26,27,30]. In a finite element study, Dyrkacz and colleagues showed significant differences in the amount of micromotion between taper sizes [31] and the increase in fretting corrosion might even be larger if materials with a lower modulus of elasticity are used for the stems, e.g. Ti6Al4V or TMZF vs. CoCr29Mo [27]. The reduced flexural rigidity and usage of titanium for femoral stems has been identified as a potential cause for the increased incidence of corrosion in current THA designs over a wide range

of retrieval studies [10,32,33], while the effect of smaller taper sizes as a risk factor for early revision is discussed controversially [29,34]. As a change of geometry does not only affect the bending and torsion rigidity properties, but also the ROM, the reduction of the taper size to obtain an increased ROM, results in a trade-off in rigidity. A balance between flexural rigidity of the junction and impingement-free ROM must be achieved [35]. However, the influence of reduced flexural rigidity and elastic modulus of the stem on corrosion risk may also depend on other factors, e.g. the head material [32].

Currently the variety of taper sizes in clinical use is still large. The range covers taper sizes of 8/10 mm up to 14/16 mm. The Exeter V40 (Stryker) and the Corail (Depuy Synthes) are the most frequently used femoral stems for total conventional hip replacement in Australia (AOA, 2017). The V40 taper shows significantly smaller dimensions than the 12/14 taper of the Corail stem. Besides the taper geometry, large variations can be seen in the design of the neck. Either of these two parameters can have an impact on micromotion and fretting corrosion and is therefore of great clinical relevance. The purpose of this study was to clarify whether lower flexural rigidity of the taper and the neck geometry increases the amount of micromotion at the head-stem taper junction under physiological loading conditions.

2. Materials and Methods

2.1 Materials and surface geometry

Based on the design of two clinically successful stem designs (Accolade TMZF, Stryker, Kalamazoo, MI, US; Corail, DePuy Synthes, Raynham, MA, US), five different models of the stem taper and the proximal stem section were manufactured from Ti6Al4V (Figure 3; n = 3 each). Geometries of the Accolade and Corail stems were captured via 3D surface scanning technique (Handyscan 700, Creaform, Lévis, Canada; 480,000 data points/s, measurement temperature 21 °C) with a resolution of 0.05 mm and an accuracy of 0.03 mm. This accuracy resulted in an error of less than 1/1000 of the neck geometry (Figure 4). The 3D surface scans were further edited to remove minor surface irregularities which occurred during the scanning process (spatial filter; Geomagic Studio, Geomagic, Morrisville, NC, United States). The male stem taper geometries of the Accolade and Corail were additionally acquired using a tactile coordinate measuring machine to increase accuracy (1.7 µm; Crysta Apex S 574, Mitutoyo Germany, Neuss, Germany).

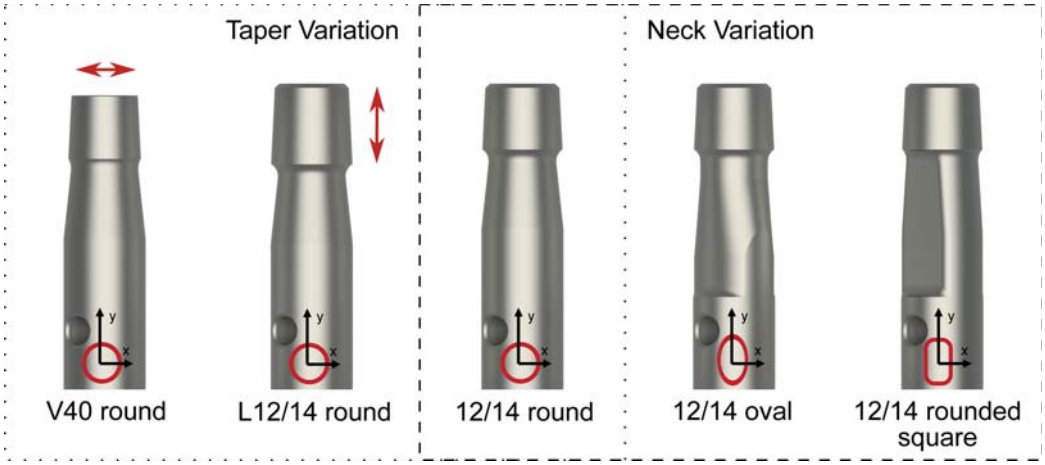

Figure 3: Overview of custom-made proximal stem and stem taper designs. The transversal bore was added for handling purposes during disassembly. The round proximal stem design was used to investigate the influence of taper design (12/14, V40, long 12/14). The 12/14 taper designs were used to investigate the influence of proximal stem geometry (oval, rounded, rounded square).

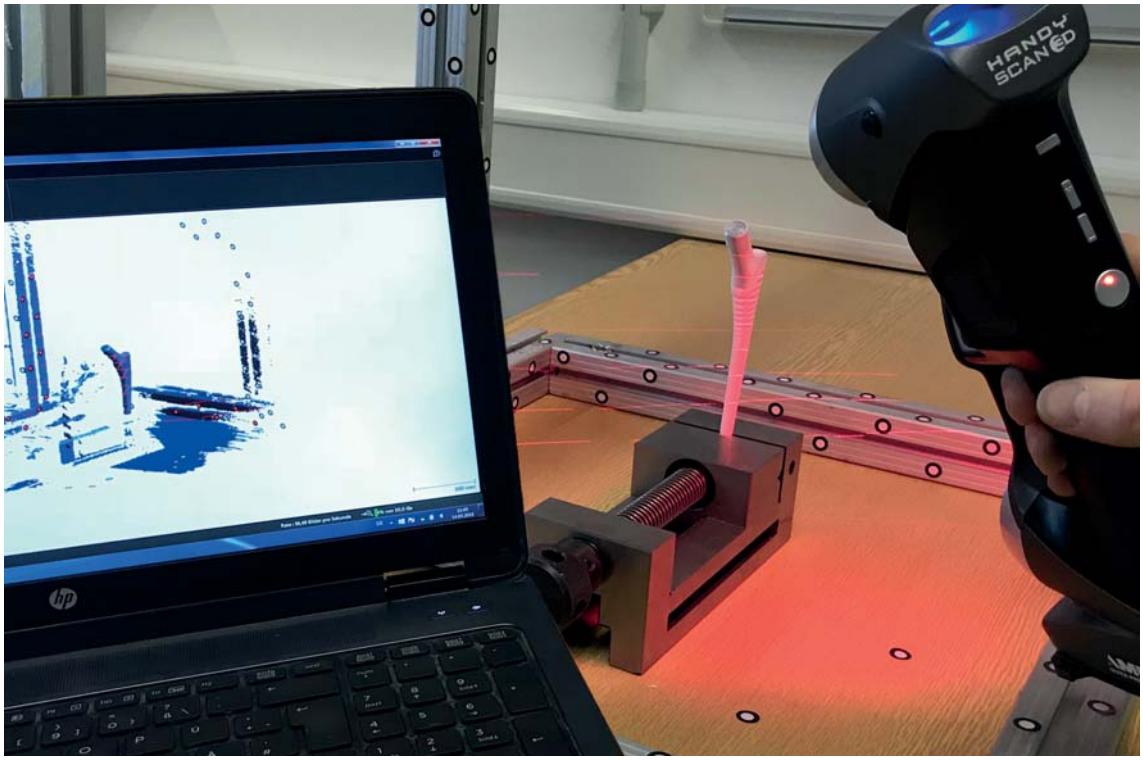

Figure 4: Setup for the digitalization of the prosthesis geometry using a 3D scanner.

The influence of three different taper designs was determined based on a round proximal stem geometry (Ø = 14 mm): a 12/14 taper, a V40 taper and a long 12/14 taper (Figure 3, Table 1). Three different proximal stem designs consisting of the Accolade (oval), the Corail (rounded square) and a custom design with a round proximal geometry, all with a 12/14 taper, were used to investigate the influence of proximal stem design (Figure 3). The use of custom-manufactured models rather than original prostheses was chosen to facilitate the systematic analysis of the influence of geometric differences in the taper and

proximal stems regions while neglecting factors such as elastic modulus, taper surface structure or taper angle.

Table 1: Geometrical properties for the 5 custom-made models (n=3). The reference cross sections of the neck geometry were taken 20 mm distally from the proximal taper surface (according to figure 1).

Specimen Type	Neck geometry			Male taper geometry			Head
	Cross section	a [mm]	b [mm]	Proximal Ø [mm]	Angle [°]	Length [mm]	Type
12/14	round	12.98	-	12.550±0.001	2.822±0.002	11.2	M-Spec (DP)
V40	round	13.05	-	11.300±0.001	2.828±0.001	10.8	LFiT V40 (ST)
L12/14	round	12.43	-	12.550±0.002	2.823±0.003	13.7	M-Spec (DP)
12/14	oval	12.60	11.50	12.550±0.001	2.824±0.002	11.2	M-Spec (DP)
12/14	rounded square	13.23	9.30	12.550±0.001	2.827±0.003	11.2	M-Spec (DP)

2.2 Computation of flexural rigidity

Flexural rigidity is commonly determined based on either the diameter of the distal taper contact [27–29,36,37] or the geometric taper centroid diameter [38] for a specific position and a fixed diameter. In the present study, a continuous calculation of rigidity was performed along the taper axis for the taper and neck region. Hence, the calculation of the flexural rigidity is carried out in lateral and central direction at every single position of the whole geometry of the prosthesis (Figure 5). To achieve this, the CAD models were converted into surface models and post-processed with Matlab (2017b, The Mathworks,

Natick, MA, United States). Surface geometries were then converted into a point cloud. Starting at the proximal taper plane, the local second moment of inertia was determined for any cross-section with an increment of 0.5mm moving in distal direction along the taper axis. The local second moment of inertia (I) was then multiplied by the elastic modulus (E) to report the flexural rigidity (FR) of the proximal stem region. The elastic modulus used for the models was 120 GPa. To investigate the influence of material, a FE model was also created for the oval V-40 model using the material properties of TMZF (elastic modulus: 85GPa), the material from which the Accolade stem is made.

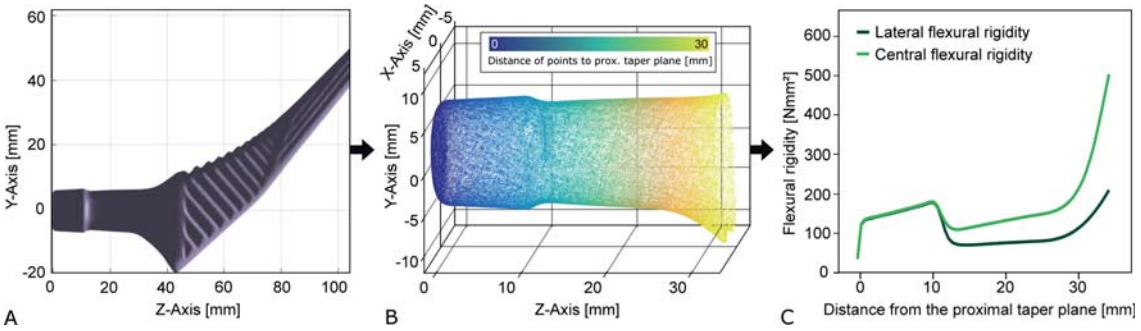

Figure 5: Calculation of the flexural rigidity for the taper and neck geometry. A 3D-scan of the prosthesis was obtained (a) and the corresponding point cloud derived (b). The precise geometry of the taper region was further gathered by a coordinate measuring machine. The flexural rigidity was calculated for each cross section of the prosthesis starting from the proximal plane.

2.3 Relative motion measurement

Prior to testing, each stem was cleaned and assembled quasi-statically (F = 2000 N) with a metal ball head along the taper axis (ISO 7206-10; Z010, Zwick/Roell, Ulm, Germany). For the V40 taper, L-Fit V40 heads (Stryker), for the 12/14 tapers, M-SPEC Metal heads (DePuy Synthes), both CoCr29Mo (Ø 36 mm) were used. The distal part of the models was fixed in a three-jaw lathe chuck (ZE-6353-125, Mack Werkzeuge, Sontheim Brenz, Germany) and inclined according to physiologically loading angles (10 ° adduction and 9 ° flexion; ISO 7206-4). Force-controlled cyclic loading (1 Hz) was applied via a PE piston (22 mm contact diameter) to the head using a servo-hydraulic testing machine (1 Hz; MiniBionix II, MTS, Eden Prairie, MN, USA). A total of three activity levels were simulated that reflect situations of daily living [25]: F_{L1} = 230-2300 N (walking, 1 h), F_{L2} = 230-4300 N (stair climbing, 0.5 h) and F_{L3} = 230-5300 N (stumbling, 0.5 h).

The relative motion between the head and the stem component was measured contactless, utilizing six eddy-current sensors (Type ES05(78), MicroEpsilon, Ortenburg, Germany, resolution 50 nm). The sensors and corresponding reflectors (St37) were mounted into two holders that were rigidly fixed to the head and the models. The distance between sensors and their respective reflectors was continuously measured (Figure 6a). Upon loading the corresponding relative motion was captured as a change in distance (measurement range 500 µm). Relative motion at the head center was computed using a coordinate transformation. Further details on the measurement setup are described elsewhere [39]. All measurements were performed within a temperature-controlled chamber containing four PID-controlled ceramic heat radiators (30±0.1 °C; Quantrol

LC100, Jumo, Fulda, Germany). After testing, the pull-off forces of the heads were measured according to ISO 7206-10.

Testing of original Corail and Accolade prostheses was also performed to validate the TMZF FE-model of the Accolade proximal stem and taper as well as the manufactured model of the Corail proximal stem and taper. The distal parts of the stems were fixed at the resection plane using custom-made prosthesis-specific mounts (Figure 6b), designed in accordance with ISO 7206-6.

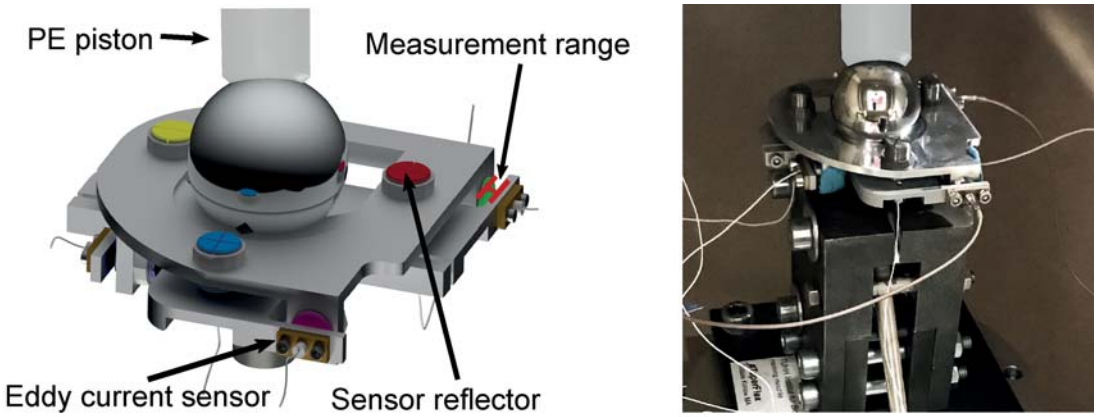

Figure 6: Experimental setup used to measure relative motion between the head and stem. Six eddy current sensors are placed around the taper junction (a). Custom-designed holders were used to mount the prostheses in accordance with ISO standards (b).

2.4 Micromotion

When using non-destructive methods, it is only possible to determine the relative motion between the head and the stem, which is a combination of elastic deformation and micromotion. Micromotion can consequently be determined by subtracting the elastic deformation from the measured relative motion. Relative motion was therefore measured for “near”-monoblocks of two of the models investigated (S12-14 round and V40 round). “Near”-monoblocks were produced by assembling respective heads and models with a very high axial assembly force of 70 kN (SCHENK, PC400M, Darmstadt, Germany). Higher forces could not be used since they caused plastic deformation of the models. Measured relative motion of the “near”-monoblocks consist nearly of the pure elastic deformation. After subtraction of the elastic deformation, pistoning, lateral and central rocking micromotion were combined to the total translational micromotion (Euclidean norm), while total rotational micromotion is described by the norm of screwing, central and lateral toggling (Figure 7).

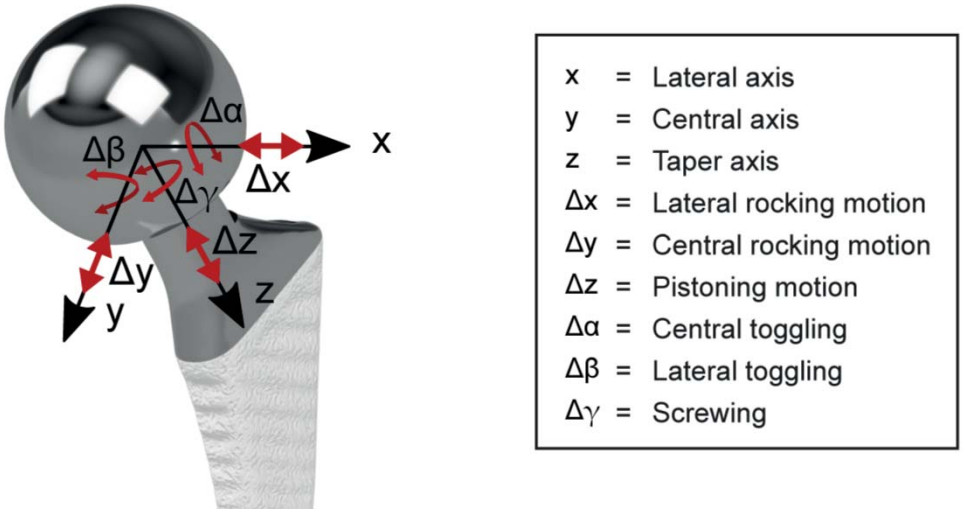

Figure 7: Notation for the directions of the measured relative motion at the head-stem junction with respect to a coordinate system fixed at the head center.

2.5 Finite element model

A total of 10 numerical models were created (ABAQUS 6.14-2, Dessault Systèmes, Vélizy-Villacoublay, France), 5 of those representing the modular head-stem taper junction with the individual stem-adapter designs (Figure 3) and 5 to simulate corresponding monoblock versions analogue to the experimental study. In addition, the V40 models were simulated with two different material properties (Ti6Al4V: 120 GPa, TMZF: 85 GPa).

Each model consisted of the head and the proximal stem model as well as a simplified structure of the holders using beam elements (10x10 mm) for improved computational performances. The model was orientated analogue to the experimental setup fulfilling the

ISO requirements. Sinusoidal load was applied over two cycles for each activity level due to the quasi-static simulation. Tangential behavior was used to discretize the interaction including finite sliding with a penalty friction formulation and a friction coefficient of $\mu = 0.3$. All implant geometries were meshed with linear hexahedron elements (C3D8R). The contact area of the male taper (slave surface) was meshed with a seed size of 0.4 mm and of the female taper (master surface) with 0.8 mm. An increased mesh size was chosen for areas without surface contact. An analysis of convergence was performed to ensure a suitable mesh size. Monoblocks were modelled by rigidly combining the head and stem using a Boolean function. The ball head was translated on the male taper by the amount of secondary seating obtained from its corresponding modular model. Head (CoCr29Mo: 210 GPa) and stem material were reassigned to match their original geometries as before merging.

2.6 Statistical analysis

Pull-off force, total translational and rotational relative motion were compared statistically between activity level and stem or taper design, using a parametric analysis (one-way analysis of variance (ANOVA)) and post hoc test (Tukey), or a non-parametric analysis (Kruskal-Wallis) with the probability of a Type I error set to $\alpha = 0.05$ (SPSS Statistics 23; IBM Corp., Armonk, NY). All results are reported as mean and SD.

3. Results

311 *3.1 Flexural rigidity of the taper and the neck region*

312 The maximum taper rigidity for the 12/14 round taper was computed to be 188 Nm^2,
313 whereas the long version of the 12/14 round taper had a slightly greater taper rigidity of
314 194 Nm^2. (Figure 8a). The V40 round male taper showed a maximum computed taper
315 rigidity of 126 Nm^2. All three taper designs showed the same distribution of flexural
316 rigidity within the distal neck region. For the different stem geometries, taper rigidity was
317 constant with a magnitude of 188 Nm^2 since the taper was similar for all geometries
318 (Figure 8b). The round proximal stem cross section showed similar flexural rigidities in
319 both bending directions. An oval neck region led to more flexible properties in lateral
320 direction compared to the central bending direction (-70 %). Models with rounded square
321 neck region proved to be most flexible in lateral direction when compared to the other
322 models (-100 %). The lower lateral flexural rigidity of the neck geometry was consistent
323 with higher displacements observed in the finite element model (Figure 9).

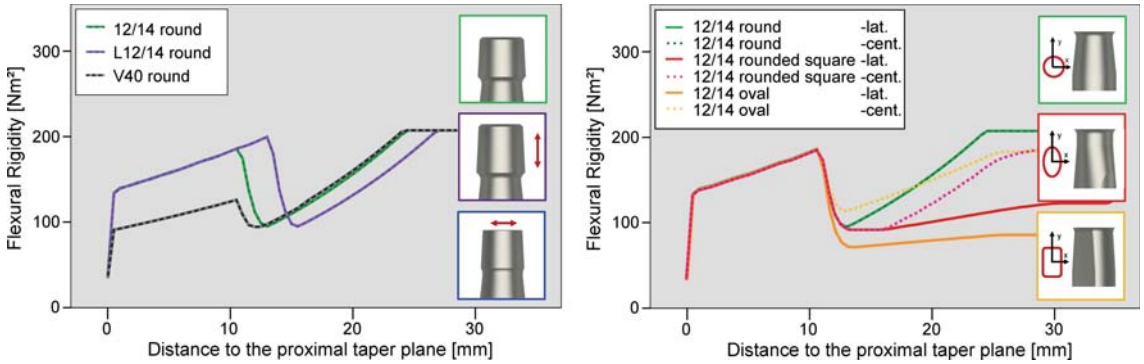

Figure 8: Flexural rigidity computed with a constant elastic modulus of 120MPa for the different taper designs (a) and neck variations (b). Proximal stem models were clamped at 30mm distance from the proximal taper plane.

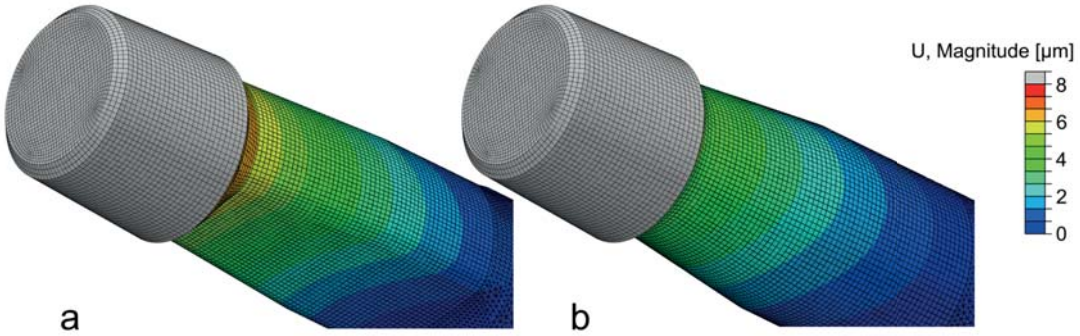

Figure 9: Finite element model of the proximal neck and taper region for the 12/14 rounded square (a) and 12/14 round neck geometry (b). The lower lateral flexural rigidity is highlighted by higher displacements in the neck.

3.2 Total translational relative motion

Increasing activity levels caused a marked increase of total translational relative motion (Table 2; $p < 0.001$). Total translational relative motion of the 12/14 round model during walking was 16±0.6 µm. For the smaller V40 round model, an increase to 19.2±0.9 µm was seen ($p < 0.001$; all activity levels). The increased taper length of the long L12/14 round model led to a significant increase of total translational relative motion compared to the reference taper (22.9±0.4 µm; $p < 0.001$; all activity levels).

The rounded square neck geometry showed an enlarged total translational relative motion compared to the round geometry (17.3±1.1 µm; $p < 0.001$). A similar difference was found for the oval neck design (18.3±0.2 µm; $p < 0.001$; all activity levels).

The results for the original Corail stem and the corresponding custom-made model (12/14 rounded square) showed slightly lower relative motion for the original stem during walking (15.0 µm vs. 17.3 µm). The numerical results matched the experimental results within 10 % tolerance. For the activity level stumbling, a difference of only 0.05 % was achieved (Table 2).

Table 2: Experimentally and numerically determined relative motion of the different models.

Activity level [N]		Relative motion [µm]													
		12/14 round		L12/14 round		V40 round		12/14 oval		12/14 rounded square		12/14 round "near"-Monoblock		V40 round "near"-Monoblock	
		Exp.	Num	Exp.	Num	Exp.	Num	Exp.	Num	Exp.	Num	Exp.	Num	Exp.	Num
FL1	230-2300	16.1 ± 0.6	17.4	22.9 ± 0.4	19.4	18.9 ± 0.9	19.9	18.3 ± 0.2	20.5	17.3 ± 1.1	18.8	14.7	16.5	17.2	17.7

FL2	230-4300	33.1 ± 0.8	33.7	46.3 ± 1.0	37.6	39.5 ± 1.1	38.2	37.4 ± 0.7	39.8	36.6 ± 0.4	36.7	30.0	32.5	35.9	34.9
FL3	230-5300	41.5 ± 0.8	41.7	58.1 ± 1.4	46.6	49.8 ± 1.3	47.1	47.2 ± 1.0	49.4	46.0 ± 0.3	45.5	37.8	40.5	44.8	43.5

352

353

354 *3.3 Total translational and rotational micromotion*

355 Total translational and rotational micromotion in the junction (without elastic
356 contribution of the neck) was higher for increasing activity levels (Figure 10). For the
357 12/14 round reference model a total translational micromotion was computed within the
358 range of 2.2-2.8 μm (walking-stumbling) and 0.003-0.010 ° for rotational motion. Similar
359 amounts of total micromotion were computed for the 12/14 rounded square and 12/14
360 oval model (2.2-2.8 μm; 0.004-0.010°). Prolongation of the taper (L12/14 round) led to
361 increased total translational and rotational micromotion compared to the reference taper
362 (2.3-3.0 μm and 0.005-0.012 °). Models with V40 taper design exhibited increased total
363 translational and rotational micromotion in the range of 2.9-4.5 μm (V40 round) and 3.3-
364 5.2 μm (V40 round TMZF, Figure 10a-b), respectively 0.002-0.016 ° and 0.006-0.022 °.

365

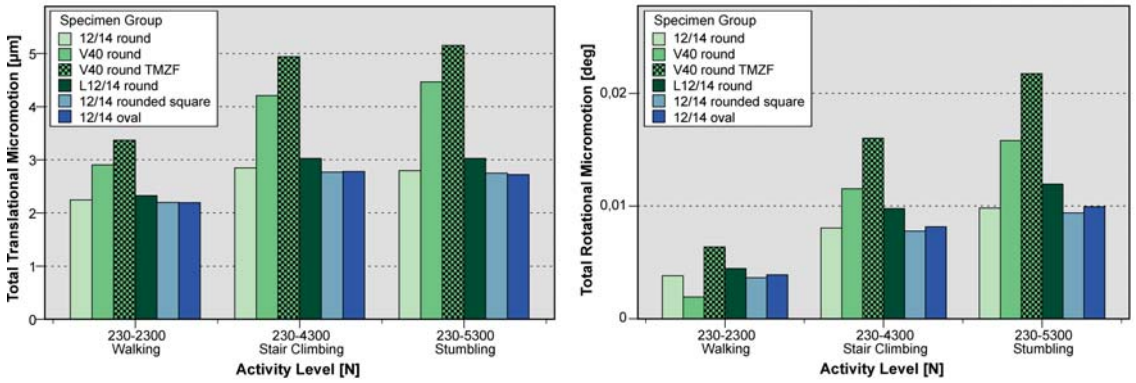

Figure 10: Total translational (a) and rotational (b) micromotion of the different models for the three activity levels.

3.4 Rocking and pistoning micromotion

By separating the total translational micromotion into rocking motion (radial to the taper axis) and pistoning motion (in axis of the taper) smaller taper diameters exhibited an increase in rocking motion of about 300 % for all activity levels. Taper length or neck geometry did not show any differences in rocking micromotion (Figure 11a).

Pistoning motion was observed in the range of -2.2 µm to -2.8 µm for the models using the 12/14 taper designs (12/14 round, rounded square, oval). Long tapers showed a slight increase in pistoning micromotion (-2.3 µm to -3.0 µm). No effect of reduced taper diameter size (V40 round) on the amount of pistoning micromotion could be detected during walking. Pistoning micromotion increased by 15 % compared to the reference model for higher activity levels. Lower elastic modulus resulted in an increase of

pistoning micromotion of approximately 20 % compared to the same taper design with the conventional material properties (Figure 11b).

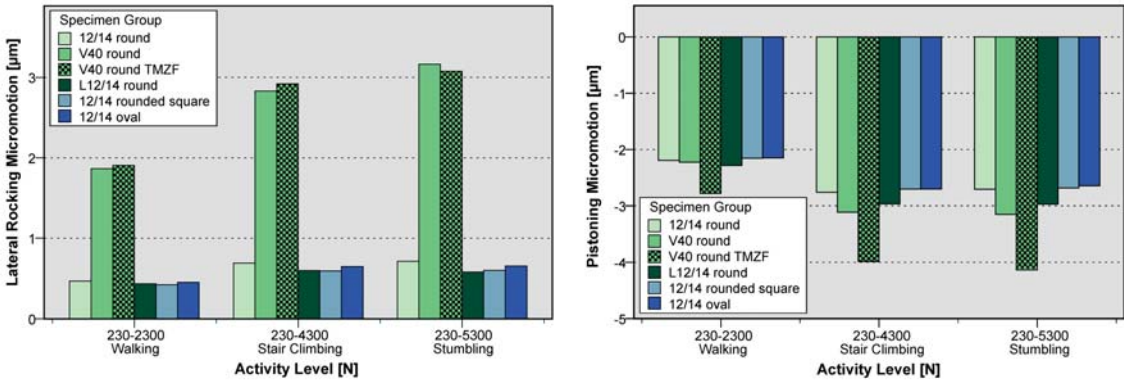

Figure 11: Rocking (a) and pistoning (b) micromotion of the different models for the three activity levels.

3.5 Taper strength analysis

The pull-off force for the models with the 12/14 taper and the long 12/14 taper design was similar (1750±238 N re. 1679±97 N; $p = 1.00$). The V40 taper design showed a slightly elevated pull-off force (2025±115 N) compared to the 12/14 taper designs ($p = 0.238$).

4. Discussion

Current research suggests that in-vivo material loss within modular taper junctions is attributable to mechanically assisted crevice corrosion (MACC; [40]). MACC can occur if two prerequisites are fulfilled: the presence of fluid in the body and micromotion between two mating surfaces [41]. The micromotion between the two surfaces can damage the passivation layer of the metal surface and leave the surface temporarily exposed to the surrounding body fluids. As a consequence, the prevention of micromotion is the key concept to minimize the impact of MACC [42].

Low-elastic modulus titanium composite stems (e.g. TMZF) were introduced to decrease stress shielding of the bone and improve femoral remodeling [43]. This beneficial characteristic, however, comes with drawbacks: the decreased elastic modulus may foster the expression of micromotion [36,39,44], which is confirmed in the present study. Another drawback of TMZF is the limited wear resistance under loading [45]. This is further supported by reports, showing less clinical adverse reactions for Ti6Al4V 11/13 tapers vs. TMZF V40 [30]. For bi-modular prostheses, TMZF stems in combination with CoCr neck adapters were shown to exhibit extensive surface damage and CoCr material loss, again supporting that material is crucial for early implant failure [46,47].

The 30 % lower elastic modulus of TMZF (TMZF with 85 GPa vs. Ti with 120 GPa) resulted in an increase of 15 % in translational micromotion and of 30% in rotational micromotion (toggling). Separation of the translational micromotion showed that the influence of lower modulus of elasticity on micromotion was most prominent for

415 pistoning motion (+30 % vs. Ti6Al4V; Figure 11) while rocking motion was not as
416 extensively expressed (<5 %). These findings corroborate with other publications
417 reporting twice the amount of pistoning motion for TMZF compared to Ti at a loading
418 amplitude of 3200 N (Accolade I: 12.5 µm vs. Accolade II: 6.6 µm; [48]). The smaller
419 micromotion values in the present study are due to the compensation of the elastic
420 component from the relative motion by using numerical simulations.
421 Fretting corrosion within taper interfaces is a multifactorial problem that is affected not
422 only by material choice, but also patient-specific parameters, handling by the surgeon and
423 implant design [5,49]. The later one has been addressed in various reports, identifying the
424 femoral stem taper flexural rigidity as a major factor for fretting corrosion [27–29,36]. In
425 a retrieval analysis Arnholt and colleagues showed for total knee arthroplasties that the
426 flexural rigidity of female tibial tapers was negatively correlated with fretting corrosion
427 scores, while patient factors such as implantation time, patient weight and age showed no
428 influence on corrosion [36]. Moreover, Higgs and colleagues showed in a retrieval study
429 that stiffer tapers (range: 84.5-402.6 Nm^2) exhibit less fretting damage, while the taper
430 size (C taper vs. V40) had no effect on head fretting [29]. In contrast, the more flexible
431 11/13 taper sizes have been reported to show significantly higher taper fretting scores
432 compared to 12/14 sizes even for a single manufacturer [30]. Consistent with these
433 findings, the rocking micromotion was more than 300 % higher for the V40 taper design
434 compared to 12/14 sizes in the present study. The same trend can been observed for the
435 toggling motion (+30 % rotational micromotion [50]). Toggling can presumably lead to

436 an cyclic opening and widening of the gap and subsequent fluid ingression [42] as well
437 as severe plastic deformation and wear [51]. Increased corrosion has been found at the
438 distal section of the taper region, possibly due to a combination of fluid ingress and
439 enlarged bending moments [30], resulting in some cases even in catastrophic failure of
440 the implant due to plastic deformation and abrasive wear of the taper surface [5,46].
441 Reduced taper length (mini vs. standard taper) was found to have a negative impact on
442 fretting corrosion risk [52]. This finding is supported by the lower rocking motion
443 observed for the long version of the 12/14 taper (-10 %). The larger contact area in the
444 long version might limit the bending loads via geometrical constraints and increased
445 flexural rigidity. The higher pistoning motion for the long taper version might be
446 explained by the reduced contact pressures as a consequence of the extended contact area.
447 However, in this study, no differences in pull-off force were noticed that might be caused
448 by lower contact pressures and higher contact areas for the long taper design compared
449 to regular sized tapers. Fretting scores may vary to a great extent even for identical taper
450 types due to variations in taper length, as they are adapted by manufacturers (e.g. range
451 for 12/14 tapers: 10.8-14.2 mm; [7]). In the case of short tapers, the head-stem taper axes
452 might be tilted due to higher bending moments resulting in an ongoing head rocking. In
453 contrast, the increased pistoning of long tapers might be of secondary importance as no
454 bending moments and widening of the gap are induced during translational motion.
455 Whether a head-taper interface is more likely to be negatively affected by explicit head
456 rocking or pistoning is still unclear. Retrieval studies show extensive damage pattern on

457 opposite areas of the taper suggesting such a toggling effect [50]. In contrast, only minor
458 differences between round, oval and rounded square designs regarding toggling motion
459 were observed even for large variations in flexural rigidity of the neck designs. This could
460 be different for heads with high offsets due to the higher bending and friction moments.
461 Considering the current trend towards smaller and less stiff implants [10], the impact of
462 bending moments might be even more crucial. On the other hand, the transition from
463 round to rounded square neck geometries also offered advantages by reduction of the
464 impingement risk, e.g. the original Corail neck vs. AMT Corail neck resulted in an
465 increase of +10° in flexion and +18° in extension [12].
466 Micromotion increased significantly with higher activity level, indicating that patients
467 with a high BMI are more affected by micromotion and possible implant failure [49].
468 Earlier studies indicate that fretting corrosion is directly linked to the amount of
469 micromotion and contact pressure even if no critical value for micromotion can be derived
470 [53]. The contact pressure within the taper junctions of the present study was initiated
471 with 2000 N of assembly load for all specimen. Interestingly, in some cases, micromotion
472 did not increase with higher activity levels (cyclic load of 5.300 N), which might be
473 explained by an additional seating of the head on the taper followed by less vulnerability
474 for head toggling. If physiological friction moments are present, the prevalence for head
475 toggling might even further increase and be expressed more clearly for taper junctions
476 with lower contact pressures. In consideration of the fact that BMI and total number of

477 performed THAs are increasing for most countries, the significance of micromotion and
478 taper fretting could increase further.

479 The multifactorial nature of the problem is highlighted as contradicting reports have been
480 published about the influence of single factors. Some studies did conclude that lower
481 flexural rigidity was only found for specific material combinations [32,54] or could even
482 lead to reduced damage scores [38]. These diverse findings [55] highlight the importance
483 of isolated investigations of design, handling and patient-specific factors on the
484 occurrence of MACC [8]. Retrieval studies typically address a mix of various factors such
485 as geometry, surface morphology and material issues in combination with unknown
486 parameters such as assembly and loading. The approach presented in this study using
487 custom-made parts is in contrast well suited for the investigation of isolated parameters.

488 A limitation of the present study is the simplification to the proximal geometry of a
489 prosthesis and minor deviations from the micro-grooved structure of the tapers used by
490 the manufacturers. Although geometrical parameters were kept identical to the original
491 protheses, manufacturing imperfections can have a significant impact on the quality of
492 the taper junction [56]. This is also important to consider as manufacturing tolerances
493 cannot be eliminated during an experimental study. Accordingly, those deviations cannot
494 be considered in the numerical simulation as well as the precise material properties. Those
495 values were obtained from literature, while variations in elastic modulus are known to
496 exist for titanium alloys. Moreover, the simulations conducted in this study considered

real-monoblock approaches. The experimentally tests were based on “near”-monoblocks as the crevice between the male and female taper depends on the taper angle difference.

5. Conclusion

In an attempt to increase impingement free range of motion, modern taper designs show a tendency to be thinner and shorter as traditional ones. This change reduces the rigidity of the modular taper junction [10], which has early been identified as a potential cause of fretting [27,33]. While the size, geometry and the material of the taper junction are not the only relevant factors contributing to risk of fretting corrosion [57], strong evidence has been presented that those factors are of high importance for the observed micromotion [5,8,42]. The influence of neck geometry as a risk factor was rather secondary in the present study. Favoring rounded square neck designs instead of smaller taper sizes could be an alternative to increase range of motion without enlarging the risk of fretting corrosion. The use of more elastic materials might have the similar effect as small tapers. Manufacturers should consider stiffer taper designs to avoid early implant failure.

Acknowledgements

The authors would like to thank DePuy Synthes for providing the prosthesis components.

Conflict of interest statement

All experimental studies were performed at the TUHH Hamburg University of Technology. The Institute of Biomechanics is receiving institutional support by DePuy

Synthes but not related to this study. Prof. Morlock is a consultant to DePuy Synthes and serves on speaker bureaus for Aesculap, AORecon, Ceramtec, Corin, Lima, Mathys, Peter Brehm, DePuy Synthes, Zimmer-Biomet. The other authors have nothing to declare.

Ethical approval

Not required.

Funding

None.

References

[1] Kluess D, Martin H, Mittelmeier W, Schmitz K-P, Bader R. Influence of femoral head size on impingement, dislocation and stress distribution in total hip replacement. Med Eng Phys 2007;29:465–71. doi:10.1016/j.medengphy.2006.07.001.

[2] Matsushita A, Nakashima Y, Jingushi S, Yamamoto T, Kuraoka A, Iwamoto Y. Effects of the Femoral Offset and the Head Size on the Safe Range of Motion in Total Hip Arthroplasty. J Arthroplasty 2009;24:646–51. doi:10.1016/j.arth.2008.02.008.

[3] Belvedere C, Cadossi M, Tamarri S, Lullini G, Ensini A, Cencioni A, et al. Impingement and range of motion in total hip replacement: A three-dimensional gait and video-fluoroscopic analysis. Gait Posture 2016;49:S19. doi:10.1016/j.gaitpost.2016.07.050.

[4] Werner PH, Etema HB, Wit F, Morlock MM, Verheyen CCPM. Basic principles and uniform terminology for the head-neck juncton in hip replacement. HIP Int 2015;25:115–9. doi:10.5301/hipint.5000204.

[5] Morlock M, Bünte D, Gührs J, Bishop N. Corrosion of the Head-Stem Taper Junction—Are We on the Verge of an Epidemic?: Review Article. HSS J 2017;13:42–9. doi:10.1007/s11420-016-9526-4.

[6] Willmann G. Prinzip der Konus-Steckverbindung fur keramische Kugelkopfe bei Huftendoprothesen. Mater Wiss Und Werkstofftechnik 1993;319:315–9. doi:10.1002/mawe.19930240908.

[7] Mueller U, Braun S, Schroeder S, Sonntag R, Kretzer JP. Same Same but Different? 12/14 Stem and Head Tapers in Total Hip Arthroplasty. J Arthroplasty 2017;32:3191–9. doi:10.1016/j.arth.2017.04.027.

[8] Wight CM, Lanting B, Schemitsch EH. Evidence Based Recommendations for Reducing Head-Neck Taper Connection Fretting Corrosion in Hip Replacement Prostheses. HIP Int 2017;27:523–31. doi:10.5301/hipint.5000545.

[9] Murray DW, Carr AJ, Bulstrode CJ. Which primary total hip replacement? J Bone Joint Surg Br 1995;77–B:520–7. doi:10.1302/0301-620X.77B4.7615593.

[10] Porter DA, Urban RM, Jacobs JJ, Gilbert JL, Rodriguez JA, Cooper HJ. Modern trunnions are more flexible: a mechanical analysis of THA taper designs. Clin Orthop Relat Res 2014;472:3963–70.

[11] Morlock MM, Bishop N, Huber G. Biomechanics of Hip Arthroplasty. In: Knahr K, editor. Tribol. Total Hip Arthroplast., Berlin, Heidelberg: Springer Berlin Heidelberg; 2011, p. 11–24. doi:10.1007/978-3-642-19429-0_2.

564 [12] Vidalain J-P, Selmi TAS, Beverland D, Young S, Board T, Boldt J, et al. The
565 Corail® Hip System - A Practical Approach Based on 25 Years of Experience.
566 Berlin, Heidelberg: Springer; 2011.
567 [13] Herrlin K, Selvik G, Pettersson H, Lidgren L. Range of Motion Caused by
568 Design of the Total Hip Prosthesis. Acta Radiol 1988;29:701–4.
569 doi:10.1177/028418518802900618.
570 [14] Cuckler JM, Moore KD, Lombardi Jr A V, McPherson E, Emerson R. Large
571 versus small femoral heads in metal-on-metal total hip arthroplasty. J
572 Arthroplasty 2018;19:41–4. doi:10.1016/j.arth.2004.09.006.
573 [15] Jacobs JJ, Urban RM, Gilbert JL, Skipor AK, Black J, Jasty M, et al. Local and
574 distant products from modularity. Clin Orthop Relat Res 1995;319:94–105.
575 [16] Urban RM, Jacobs JJ, Gilbert JL, Galante JO. Migration of corrosion products
576 from modular hip prostheses. Particle microanalysis and histopathological
577 findings. J Bone Joint Surg Am 1994;76:1345–59.
578 [17] Gilbert JL, Buckley CA, Jacobs JJ, Bertin KC, Zernich MR. Intergranular
579 corrosion-fatigue failure of cobalt-alloy femoral stems. A failure analysis of two
580 implants. JBJS 1994;76:110–5.
581 [18] Cooper HJ, Della Valle CJ, Berger RA, Tetreault M, Paprosky WG, Sporer SM,
582 et al. Corrosion at the Head-Neck Taper as a Cause for Adverse Local Tissue
583 Reactions After Total Hip Arthroplasty. J Bone Jt Surgery-American Vol
584 2012;94:1655–61. doi:10.2106/JBJS.K.01352.
585 [19] Kwon YM, Khormaee S, Liow MHL, Tsai TY, Freiberg AA, Rubash HE.
586 Asymptomatic pseudotumors in patients with taper corrosion of a dual-taper
587 modular femoral stem MARS-MRI and metal ion study. J Bone Jt Surg - Am Vol
588 2016;98:1735–40. doi:10.2106/JBJS.15.01325.
589 [20] Gill IPS, Webb J, Sloan K, Beaver RJ. Corrosion at the neck-stem junction as a
590 cause of metal ion release and pseudotumour formation. J Bone Jt Surg - Br Vol
591 2012;94–B:895–900. doi:10.1302/0301-620X.94B7.29122.
592 [21] AOANJRR. Australian Orthopaedic Association National Joint Replacement
593 Registry (AOANJRR). Hip, Knee & Shoulder Arthroplasty: 2017 Annual Report.
594 Adelaide: 2017.
595 [22] Cook SD, Barrack RL, Baffes GC, Clemow AJ, Serekian P, Dong N, et al. Wear
596 and corrosion of modular interfaces in total hip replacements. Clin Orthop Relat
597 Res 1994:80–8. doi:10.1097/00003086-199401000-00013.
598 [23] Silva M, Shepherd EF, Jackson WO, Dorey FJ, Schmalzried TP. Average patient
599 walking activity approaches 2 million cycles per year. J Arthroplasty
600 2018;17:693–7. doi:10.1054/arth.2002.32699.

601 [24] Morlock M, Schneider E, Bluhm A, Vollmer M, Bergmann G, Müller V, et al.
602 Duration and frequency of every day activities in total hip patients. J Biomech
603 2001;34:873–81. doi:10.1016/S0021-9290(01)00035-5.
604 [25] Bergmann G, Graichen F, Rohlmann A, Bender A, Heinlein B, Duda GN, et al.
605 Realistic loads for testing hip implants. Biomed Mater Eng 2010;20:65–75.
606 doi:10.3233/BME-2010-0616.
607 [26] Gilbert JL, Buckley CA, Jacobs JJ. In vivo corrosion of modular hip prosthesis
608 components in mixed and similar metal combinations. The effect of crevice,
609 stress, motion, and alloy coupling. J Biomed Mater Res 1993;27:1533–44.
610 doi:10.1002/jbm.820271210.
611 [27] Goldberg JR, Gilbert JL, Jacobs JJ, Bauer TW, Paprosky W, Leurgans S. A
612 multicenter retrieval study of the taper interfaces of modular hip prostheses. Clin
613 Orthop Relat Res 2002:149–61.
614 [28] Kao Y-YJ, Koch CN, Wright TM, Padgett DE. Flexural Rigidity, Taper Angle,
615 and Contact Length Affect Fretting of the Femoral Stem Trunnion in Total Hip
616 Arthroplasty. J Arthroplasty 2016:1–5. doi:10.1016/j.arth.2016.02.079.
617 [29] Higgs GB, MacDonald DW, Gilbert JL, Rimnac CM, Kurtz SM, Chen AF, et al.
618 Does Taper Size Have an Effect on Taper Damage in Retrieved Metal-on-
619 Polyethylene Total Hip Devices? J Arthroplasty 2016;31:277–81.
620 doi:10.1016/j.arth.2016.06.053.
621 [30] Tan SC, Teeter MG, Del Balso C, Howard JL, Lanting BA. Effect of Taper
622 Design on Trunnionosis in Metal on Polyethylene Total Hip Arthroplasty. J
623 Arthroplasty 2015;30:1269–72. doi:10.1016/j.arth.2015.02.031.
624 [31] Dyrkacz RMR, Brandt JM, Morrison JB, O' Brien ST, Ojo OA, Turgeon TR, et
625 al. Finite element analysis of the head-neck taper interface of modular hip
626 prostheses. Tribol Int 2014;91:1–8. doi:10.1016/j.triboint.2015.01.016.
627 [32] Kurtz SM, Kocagöz SB, Hanzlik J a, Underwood RJ, Gilbert JL, Macdonald
628 DW, et al. Do Ceramic Femoral Heads Reduce Taper Fretting Corrosion in Hip
629 Arthroplasty? A Retrieval Study. Clin Orthop Relat Res 2013;471:3270–82.
630 doi:10.1007/s11999-013-3096-2.
631 [33] Jennings JM, Dennis DA, Yang CC. Corrosion of the head-neck junction after
632 total hip arthroplasty. J Am Acad Orthop Surg 2016;24:349–56.
633 doi:10.5435/JAAOS-D-15-00111.
634 [34] Nassif N, Nawabi DH, Stoner K, Elpers M, Wright T, Padgett DE. Taper design
635 affects failure of large-head metal-on-metal total hip replacements. Clin Orthop
636 Relat Res 2014;472:564–71. doi:10.1007/s11999-013-3115-3.
637 [35] Triantafyllopoulos GK, Elpers ME, Burket JC, Esposito CI, Padgett DE, Wright

638 TM. Otto Aufranc Award: Large Heads Do Not Increase Damage at the Head-
639 neck Taper of Metal-on-polyethylene Total Hip Arthroplasties. Clin Orthop Relat
640 Res 2015;[Epub ahea. doi:10.1007/s11999-015-4468-6.

641 [36] Arnholt CM, MacDonald DW, Tohfafarosh M, Gilbert JL, Rimnac CM, Kurtz
642 SM, et al. Mechanically assisted taper corrosion in modular TKA. J Arthroplasty
643 2014;29:205–8. doi:10.1016/j.arth.2013.12.034.

644 [37] Arnholt CM, MacDonald DW, Underwood RJ, Guyer EP, Rimnac CM, Kurtz
645 SM, et al. Do Stem Taper Microgrooves Influence Taper Corrosion in Total Hip
646 Arthroplasty? A Matched Cohort Retrieval Study. J Arthroplasty 2016.
647 doi:http://dx.doi.org/10.1016/j.arth.2016.11.018.

648 [38] Pourzal R, Bs DJH, Ba NQH, Urban RM, Levine BR, Jacobs JJ, et al. Does
649 Surface Topography Play a Role in Taper Damage in Head-neck Modular
650 Junctions ? Clin Orthop Relat Res 2016. doi:10.1007/s11999-016-4933-x.

651 [39] Haschke H, Jauch-Matt SY, Sellenschloh K, Huber G, Morlock MM. Assembly
652 force and taper angle difference influence the relative motion at the stem-neck
653 interface of bi-modular hip prostheses. Proc Inst Mech Eng Part H J Eng Med
654 2016;230:690–9. doi:10.1177/0954411916648717.

655 [40] Mali SA, Gilbert JL. Correlating Fretting Corrosion and Micromotions in
656 Modular Tapers: Test Method Development and Assessment. Modul. Tapers
657 Total Jt. Replace. Devices, 100 Barr Harbor Drive, PO Box C700, West
658 Conshohocken, PA 19428-2959: ASTM International; 2015, p. 259–82.
659 doi:10.1520/STP159120140136.

660 [41] Gilbert JL, Mali S, Urban RM, Silverton CD, Jacobs JJ. In vivo oxide-induced
661 stress corrosion cracking of Ti-6Al-4V in a neck-stem modular taper: Emergent
662 behavior in a new mechanism of in vivo corrosion. J Biomed Mater Res - Part B
663 Appl Biomater 2012;100 B:584–94. doi:10.1002/jbm.b.31943.

664 [42] Pourzal R, Lundberg HJ, Hall DJ, Jacobs JJ. What Factors Drive Taper
665 Corrosion? J Arthroplasty 2018;33:2707–11. doi:10.1016/j.arth.2018.03.055.

666 [43] Head WC, Bauk DJ, Emerson RH. Titanium as the material of choice for
667 cementless femoral components in total hip arthroplasty. Clin Orthop Relat Res
668 1995:85—90.

669 [44] Jauch SY, Huber G, Haschke H, Sellenschloh K, Morlock MM. Design
670 parameters and the material coupling are decisive for the micromotion magnitude
671 at the stem-neck interface of bi-modular hip implants. Med Eng Phys
672 2014;36:300–7. doi:10.1016/j.medengphy.2013.11.009.

673 [45] Yang X, Hutchinson CR. Corrosion-wear of β-Ti alloy TMZF (Ti-12Mo-6Zr-
674 2Fe) in simulated body fluid. Acta Biomater 2016;42:429–39.
675 doi:10.1016/j.actbio.2016.07.008.

[46] Buente D, Huber G, Bishop N, Morlock M. Quantification of material loss from the neck piece taper junctions of a bimodular primary hip prosthesis. A retrieval study from 27 failed Rejuvenate bimodular hip arthroplasties. Bone Jt J 2015;97B:1350–7. doi:10.1302/0301-620X.97B10.35342.

[47] Su SL, Koch CN, Nguyen TM, Burket JC, Wright TM, Westrich GH. Retrieval Analysis of Neck-Stem Coupling in Modular Hip Prostheses. J Arthroplasty 2017;32:2301–6. doi:10.1016/j.arth.2017.02.016.

[48] Swaminathan V, Scholl L, Lee R, Faizan A, Thakore M, TenHuisen K, et al. Simultaneous Hip Head-Stem Taper Junction Measurements of Electrochemical Corrosion and Micromotion: A Comparison of Taper Geometry and Stem Material. Modul. Tapers Total Jt. Replace. Devices, 100 Barr Harbor Drive, PO Box C700, West Conshohocken, PA 19428-2959: ASTM International; 2015, p. 321–35. doi:10.1520/STP159120140150.

[49] Morlock MM. The taper disaster - How could it happen? HIP Int 2015;25:339–46. doi:10.5301/hipint.5000269.

[50] Esposito CI, Wright TM, Goodman SB, Berry DJ. What is the Trouble With Trunnions? Clin Orthop Relat Res 2014;472:3652–8. doi:10.1007/s11999-014-3746-z.

[51] Bishop N, Witt F, Pourzal R, Fischer A, Rütschi M, Michel M, et al. Wear patterns of taper connections in retrieved large diameter metal-on-metal bearings. J Orthop Res 2013;31:1116–22. doi:10.1002/jor.22326.

[52] Panagiotidou A, Meswania J, Hua J, Muirhead-Allwood S, Hart A, Blunn G. Enhanced wear and corrosion in modular tapers in total hip replacement is associated with the contact area and surface topography. J Orthop Res 2013;31:2032–9. doi:10.1002/jor.22461.

[53] Baxmann M, Jauch SY, Schilling C, Blömer W, Grupp TM, Morlock MM. The influence of contact conditions and micromotions on the fretting behavior of modular titanium alloy taper connections. Med Eng Phys 2013;35:676–83. doi:http://dx.doi.org/10.1016/j.medengphy.2012.07.013.

[54] Lundberg HJ, Ha NQ, Hall DJ, Urban RM, Levine BR, Pourzal R. Contact Mechanics and Plastic Deformation at the Local Surface Topography Level After Assembly of Modular Head-Neck Junctions in Modern Total Hip Replacement Devices. Modul. Tapers Total Jt. Replace. Devices, 100 Barr Harbor Drive, PO Box C700, West Conshohocken, PA 19428-2959: ASTM International; 2015, p. 59–82. doi:10.1520/STP159120140148.

[55] Baleani M, Erani P, Bordini B, Zuccheri F, Makosa MK, De Pasquale D, et al. In vivo damage of the head-neck junction in hard-on-hard total hip replacements: Effect of femoral head size, metal combination, and 12/14 taper design. Materials

(Basel) 2017;10. doi:10.3390/ma10070733.

[56] Shareef N, Levine D. Effect of manufacturing tolerances on the micromotion at the Morse taper interface in modular hip implants using the finite element technique. Biomaterials 1996;17:623–30. doi:10.1016/0142-9612(96)88713-8.

[57] Rowan FE, Wach A, Wright TM, Padgett DE. The onset of fretting at the head-stem connection in hip arthroplasty is affected by head material and trunnion design under simulated corrosion conditions. J Orthop Res 2018;36:1630–6. doi:10.1002/jor.23813.

Figure and table legend

Table 1: Geometrical properties for the 5 custom-made models (n=3). The reference cross sections of the neck geometry were taken 20 mm distally from the proximal taper surface (according to figure 1). 14
Table 2: Experimentally and numerically determined relative motion of the different models. 23

Figure 1: Examples for the geometrical variations in the neck design of modular hip prostheses. Continuously varying cross sections with distance from the proximal taper surface. 7
Figure 2: Formation of fretting corrosion and the release of micro particles within the modular taper junction. 9
Figure 3: Overview of custom-made proximal stem and stem taper designs. The transversal bore was added for handling purposes during disassembly. The round proximal stem design was used to investigate the influence of taper design (12/14, V40, long 12/14). The 12/14 taper designs were used to investigate the influence of proximal stem geometry (oval, rounded, rounded square). 12
Figure 4: Setup for the digitalization of the prosthesis geometry using a 3D scanner.... 13
Figure 5: Calculation of the flexural rigidity for the taper and neck geometry. A 3D-scan of the prosthesis was obtained (a) and the corresponding point cloud derived (b). The precise geometry of the taper region was further gathered by a coordinate measuring machine. The flexural rigidity was calculated for each cross section of the prosthesis starting from the proximal plane. 15
Figure 6: Experimental setup used to measure relative motion between the head and stem. Six eddy current sensors are placed around the taper junction (a). Custom-designed holders were used to mount the prostheses in accordance with ISO standards (b). 17
Figure 7: Notation for the directions of the measured relative motion at the head-stem junction with respect to a coordinate system fixed at the head center. 19
Figure 8: Flexural rigidity computed with a constant elastic modulus of 120MPa for the different taper designs (a) and neck variations (b). Proximal stem models were clamped at 30mm distance from the proximal taper plane. 22
Figure 9: Finite element model of the proximal neck and taper region for the 12/14 rounded square (a) and 12/14 round neck geometry (b). The lower lateral flexural rigidity is highlighted by higher displacements in the neck. 22
Figure 10: Total translational (a) and rotational (b) micromotion of the different models for the three activity levels. 25
Figure 11: Rocking (a) and pistoning (b) micromotion of the different models for the three activity levels. 26